Naval Research Laboratory
Washington, DC 20375-5320

U.S. NAVAL RESEARCH LABORATORY

NRL/5708/MR—2023/2

Parametric Reduced Absorption Spectra for NIR-SWIR Absorbing Dyes on Paper Substrate

RACHEL VIGER, PA

JESSE DUNCAN

SCOTT A. RAMSEY

TROY MAYO

Signature Technology Office
Tactical Electronic Warfare Division

JAMES WYNNE

Materials Chemistry and Dynamics Branch
Chemistry Division

SAMUEL G. LAMBRAKOS

Computational Multiphysics Systems
Material Science and Technology Division

February 1, 2023

REPORT DOCUMENTATION PAGE

Form Approved
OMB No. 0704-0188

1. REPORT DATE *(DD-MM-YYYY)*	**2. REPORT TYPE**	**3. DATES COVERED** *(From - To)*
01-02-2023	NRL Memorandum Report	

4. TITLE AND SUBTITLE

Parametric Reduced Absorption Spectra for NIR-SWIR Absorbing Dyes on Paper Substrate

5a. CONTRACT NUMBER

5b. GRANT NUMBER

5c. PROGRAM ELEMENT NUMBER

6. AUTHOR(S)

Rachel Viger, PA, Jesse Duncan, Scott A. Ramsey, Troy Mayo, James Wynne, and Samuel G. Lambrakos

5d. PROJECT NUMBER

5e. TASK NUMBER

5f. WORK UNIT NUMBER
7542

7. PERFORMING ORGANIZATION NAME(S) AND ADDRESS(ES)

Naval Research Laboratory
4555 Overlook Avenue, SW
Washington, DC 20375-5320

8. PERFORMING ORGANIZATION REPORT NUMBER

NRL/5708/MR--2023/2

9. SPONSORING / MONITORING AGENCY NAME(S) AND ADDRESS(ES)

US Special Operations Command,
Special Operations Forces Acquisition, Technology, and Logistics
7701 Tampa Point Blvd
MacDill Air Force Base, Florida 33621

10. SPONSOR / MONITOR'S ACRONYM(S)

USSOCOM

11. SPONSOR / MONITOR'S REPORT NUMBER(S)

12. DISTRIBUTION / AVAILABILITY STATEMENT

DISTRIBUTION STATEMENT A: Approved for public release; distribution is unlimited.

13. SUPPLEMENTARY NOTES

14. ABSTRACT

This study describes construction of reduced absorption spectra for NIR-SWIR absorbing dyes on paper, which is by critical feature isolation and projection. The critical features are identified through a structural analysis of the peaks, troughs, and points of inflection in the calculated Kubelka-Munk absorption spectra, from diffuse reflectance measurements. These features are then parameterized and projected into a reduced feature subspace to effectively capture the fundamental characteristics of the absorbing dyes. The critical feature parameterization and projection supports the construction of parametric models capable of estimating dielectric functions for various dyes, substrates, and mixtures.

15. SUBJECT TERMS

Absorption spectra Parametric modeling
Feature projection

16. SECURITY CLASSIFICATION OF:			**17. LIMITATION OF ABSTRACT**	**18. NUMBER OF PAGES**	**19a. NAME OF RESPONSIBLE PERSON**
					Rachel Viger
a. REPORT	**b. ABSTRACT**	**c. THIS PAGE**	U	28	**19b. TELEPHONE NUMBER** *(include area code)*
U	U	U			(202) 279-5272

This page intentionally left blank.

Table of Contents

This page intentionally left blank.

1. Introduction

This study describes inverse spectral analysis of diffuse reflectance from NIR-SWIR absorbing dyes on a paper substrate for the estimation of dielectric response functions [1]. The calculated functions provide dielectric-response characteristics of the dyes and information on the sensitivity of their interactions with paper. Inverse spectral analysis is based on the reduction of absorption spectra by critical feature isolation and projection. The critical features are identified through structural analysis of the peaks, troughs, and points of inflection in the calculated Kubelka-Munk absorption spectra, from diffuse reflectance measurement [2-5]. These features are then parameterized and projected into a reduced feature subspace to effectively capture the fundamental characteristics of the absorbing dyes. The critical feature parameterization and projection supports construction of parametric models capable of estimating dielectric functions for various dyes, substrates, and mixtures. The IR-absorbing dyes considered in this study are characterized by robust spectral features. The inverse spectral analysis demonstrate the concept, as emphasized by reference [6], of applying Kramers-Kronig analysis to diffuse reflectance. This has significant practical value with respect to reduced effort for sample preparation (for spectroscopic analysis).

2. Kramers-Kronig Analysis of Diffuse Reflectance Spectra

The Kramers-Kronig analysis provides an estimation of dielectric responses using diffuse reflectance from materials on substrates and their absorption functions obtained using inverse-analysis. For this analysis, normalized extinction functions $\langle \alpha_N(\lambda) \rangle$ are determined by inverse spectral analysis of diffuse-reflectance spectra using the Kubelka-Munk model, i.e.

$$\langle \alpha_N(\lambda) \rangle = \frac{f_{KM}(\lambda)}{\max[f_{KM}(\lambda)]} \qquad (Eq.\,1)$$

and

$$f_{KM}(\lambda) = \frac{\left(1 - R_n(\lambda)\right)^2}{2R_n(\lambda)}. \qquad (Eq.\,2)$$

where R_n is the normalized reflectance relative to background, e.g., substrate. Before proceeding, it should be noted that the inversion procedure defined by Eqs. (1) and (2) has a specific sensitivity property with respect to NIR-SWIR absorbing dyes, and accordingly, is essentially equivalent to other inversion procedures, applied to different types of spectroscopic measurements. This sensitivity property is discussed below.

Next, an imaginary index of refraction, scaled according to the normalized extinction functions $\langle \alpha_N(\lambda) \rangle$, is calculated by

$$\langle k_N(\lambda) \rangle = \frac{\langle \alpha_N(\lambda) \rangle \lambda}{4\pi}, \qquad (Eq\ 3)$$

and a real-refractive-index change, consistently scaled, is calculated by the Kramers-Kronig relation,

$$\langle \Delta n_N(\lambda) \rangle = \frac{2\lambda^2}{\pi} P \int_0^\infty \frac{\langle k_N(z) \rangle dz}{z(\lambda^2 - z^2)}. \qquad (Eq\ 4)$$

Manuscript approved January 23, 2023.

Note that a multiplicative factor approximates the dependence on scatterer density, and that the Kubelka-Munk function in Eq. (2) is correlated with the absorbance function. Further, we assume that the wavelength integration range of Eq. (4) is incomplete, but of sufficient expanse for estimation of the real-refractive-index change $\langle \Delta n_N(\lambda) \rangle$. Sensitivity with respect to this incompleteness can be quantified by extrapolation procedures at the limits of the measured spectral range.

Continuing the analysis procedure, a scaling parameter C_s represents the dependence on scatterer density, defined by

$$\alpha_s(\lambda) = C_s \langle \alpha_N(\lambda) \rangle. \qquad (Eq\ 5)$$

Accordingly, the dependence of the complex index of refraction on scatterer density is

$$k_s(\lambda) = C_s \langle k_N(\lambda) \rangle \qquad (Eq\ 6)$$

and

$$n_s(\lambda) = n_0 + C_s \langle \Delta n_N(\lambda) \rangle. \qquad (Eq\ 7)$$

Numerical integration of Eq. (4) uses methods described in references [7-9] and references therein. Our spectral-reduction procedure entails the decomposition of $\langle \alpha_N(\lambda) \rangle$ in terms of reduced basis-function expansions, consisting of Lorenztian functions. Thus the integration defined by Eq. (4) is performed analytically by Hilbert transformation of analytic functions. Accordingly, letting

$$\langle \alpha_N(\lambda) \rangle = \lambda \sum_{k=1}^{N_k} \left(\frac{A_k}{\lambda_k} \right) \frac{(\gamma_k/2)^2}{(\lambda - \lambda_k)^2 + (\gamma_k/2)^2} \quad , \qquad (Eq. 8)$$

it follows that

$$\langle k_N(\lambda) \rangle = \frac{\lambda^2}{4\pi} \sum_{k=1}^{N_k} \left(\frac{A_k}{\lambda_k} \right) \frac{(\gamma_k/2)^2}{(\lambda - \lambda_k)^2 + (\gamma_k/2)^2} \qquad (Eq. 9)$$

and

$$\langle \Delta n_N(\lambda) \rangle = \frac{\lambda^2}{4\pi} \sum_{k=1}^{N_k} \left(\frac{A_k}{\lambda_k} \right) \frac{(\gamma_k/2)(\lambda - \lambda_k)}{(\lambda - \lambda_k)^2 + (\gamma_k/2)^2} \quad . \qquad (Eq. 10)$$

3. Spectral Reduction and Critical Feature Projection

The key features of the dyes, including their absorption peaks and troughs, can be characterized within a dimensionally reduced space using concepts from principle-component analysis (PCA) [10]. This method allows the full spectral data to be projected into a smaller subspace of spectral components while still maintaining the essence of the critical features – such as the peak wavelengths, peak heights, and inflection points. The characterization of the complex absorption behavior within simplified critical feature vectors can support further analysis of the key absorption characteristics and the potential dye mixture interactions. Additionally, this simplified parametric subspace can support the construction of approximate effective medium models capable of estimating reflectance from dyed substrates.

4. Case-Study Analyses

The critical feature isolation and projection was performed for 13 NIR-SWIR absorbing COTS dyes deposited on paper. The dyes chosen for analysis have maximum-absorption wavelengths in either the NIR or SWIR bands, with appreciable spectral features extending into the visible spectrum. Reference [11] describes the procedures used for sample preparation, and reflectance-spectrum measurements. For this study, these dyes are designated according to their maximum absorption wavelengths, using the designation "KM-Maximum-Absorption-Wavelength," similar to references [12,13], where chemical formulae for these dyes are given. For each of these results, the absorption spectra was calculated from diffuse reflectance measurements using the normalized Kubelka-Munk inverse analysis method.

KM-720

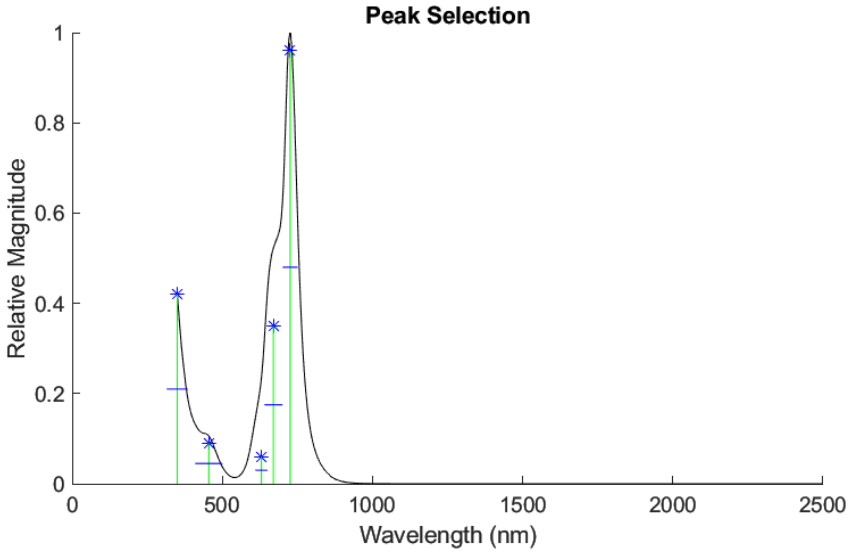

Figure 1: KM-720 absorption spectra and peak characterization.

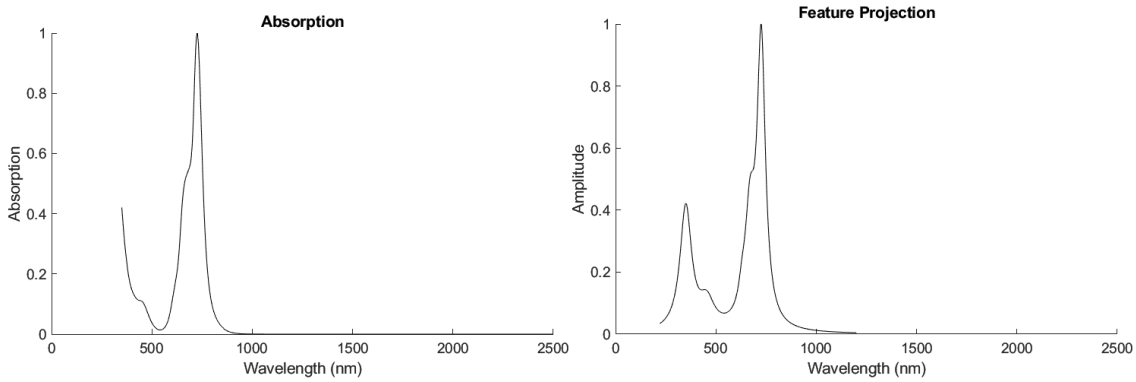

Figure 2: KM-720 comparison between the original Kubelka-Munk absorption spectra and the subspace feature projection.

Table 1: KM-720 Critical Peak Parameters

Wavelength	Peak Amplitude	Full-Width Half-Height
350	0.42	70
455	0.09	90
630	0.06	40
670	0.35	60
726	0.96	50

KM-775

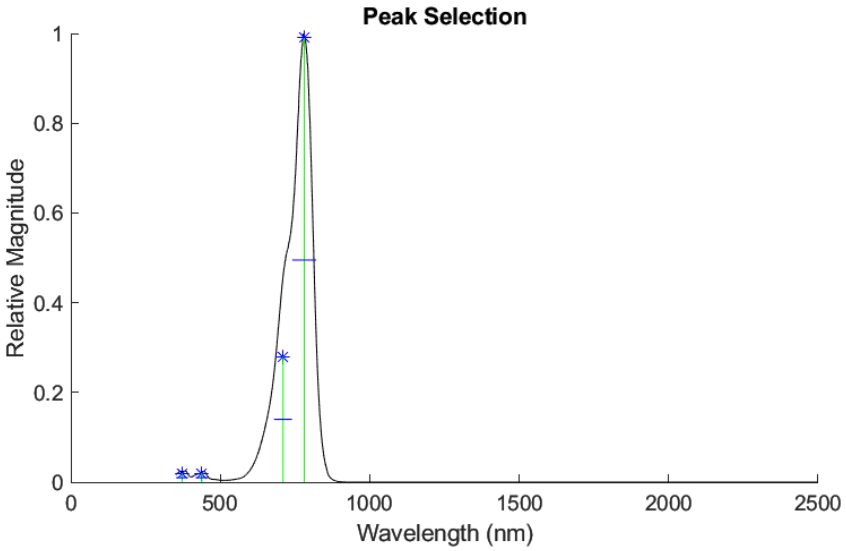

Figure 3: KM-775 absorption spectra and peak characterization.

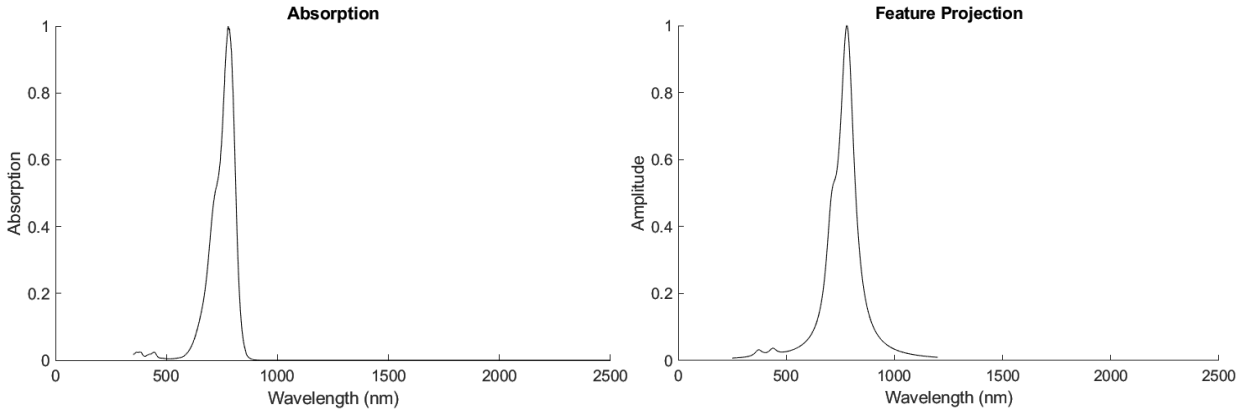

Figure 4: KM-775 comparison between the original Kubelka-Munk absorption spectra and the subspace feature projection.

Table 2: KM-775 Critical Peak Parameters

Wavelength	Peak Amplitude	Full-Width Half-Height
372	0.02	40
438	0.02	40
710	0.28	60
781	0.99	80

KM-778

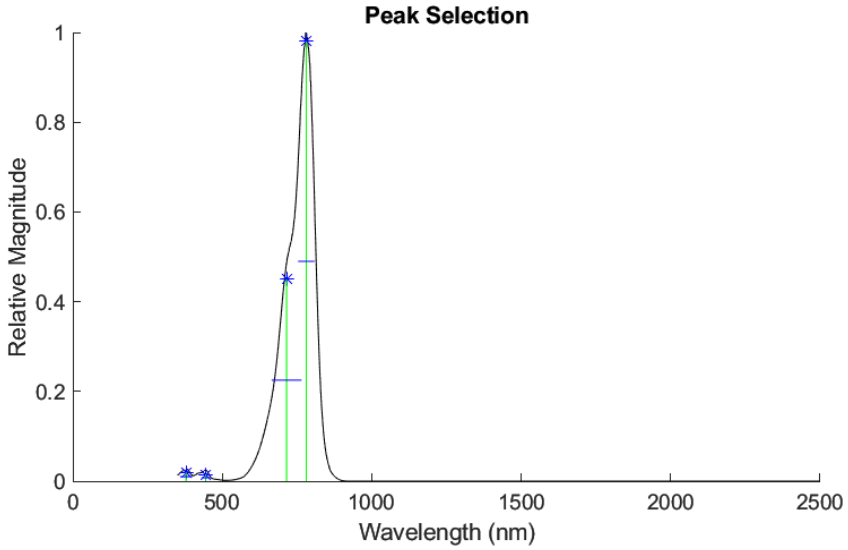

Figure 5: KM-778 absorption spectra and peak characterization.

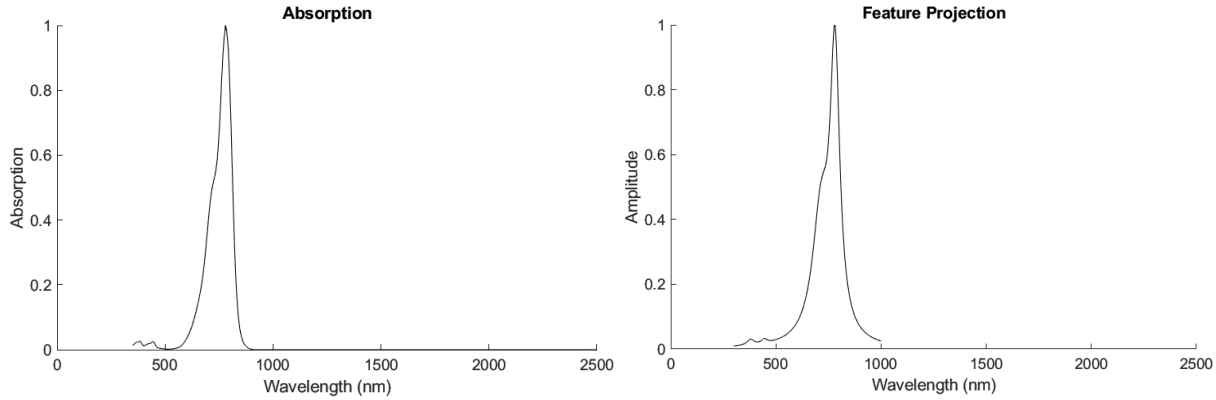

Figure 6: KM-778 comparison between the original Kubelka-Munk absorption spectra and the subspace feature projection.

Table 3: KM-778 Critical Peak Parameters

Wavelength	Peak Amplitude	Full-Width Half-Height
379	0.02	40
445	0.015	30
715	0.45	100
781	0.98	55

KM780

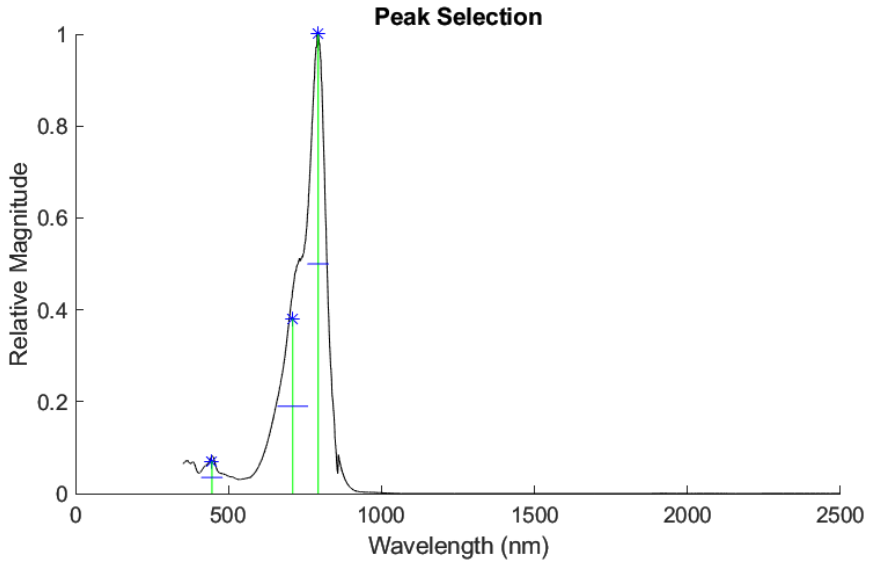

Figure 7: KM-780 absorption spectra and peak characterization.

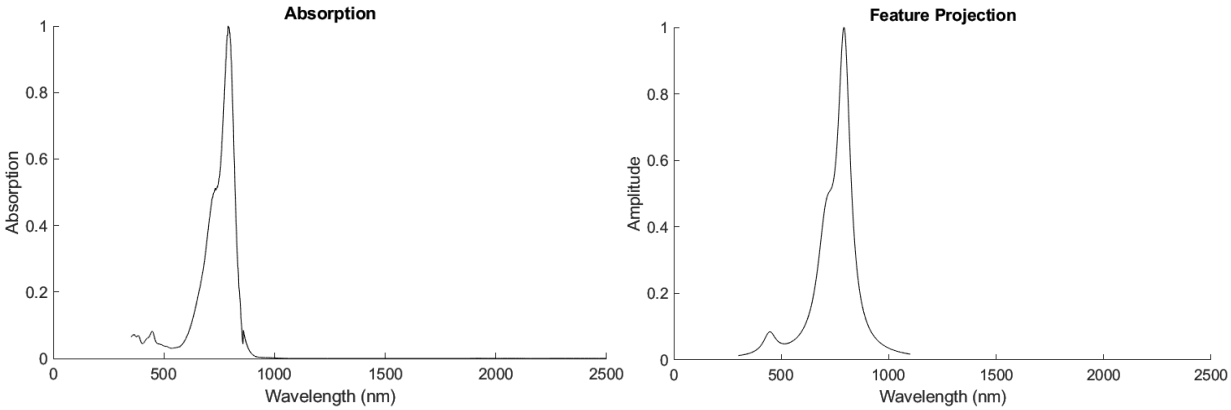

Figure 8: KM-780 comparison between the original Kubelka-Munk absorption spectra and the subspace feature projection.

Table 4: KM-780 Critical Peak Parameters

Wavelength	Peak Amplitude	Full-Width Half-Height
446	0.07	70
710	0.38	100
793	1	70

KM-825

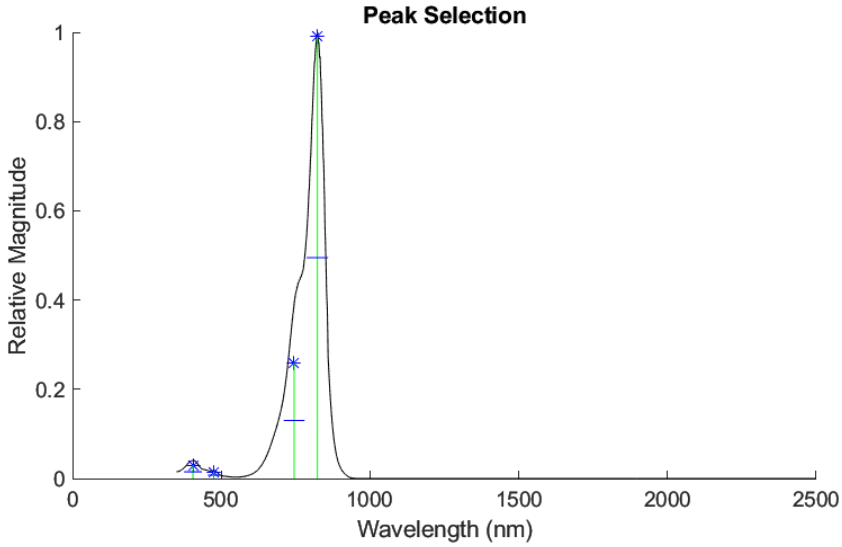

Figure 9: KM-825 absorption spectra and peak characterization.

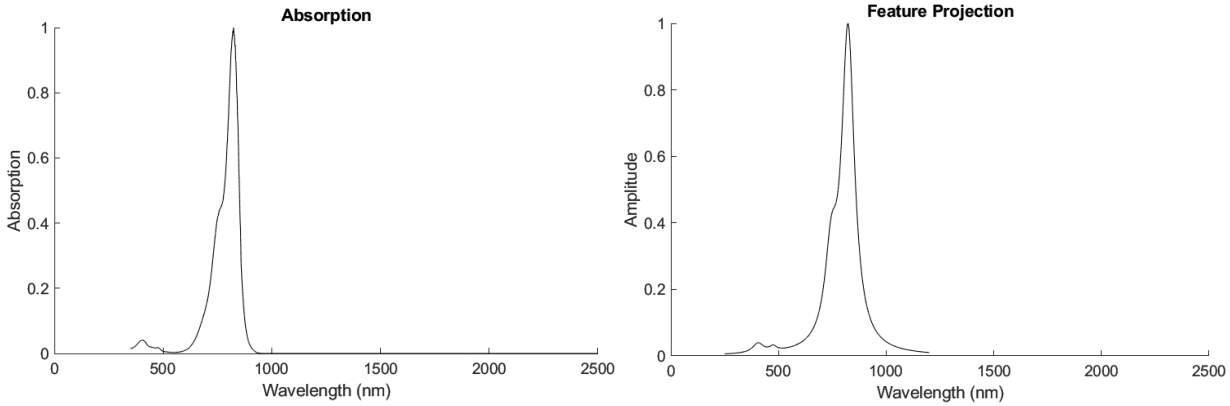

Figure 10: KM-825 comparison between the original Kubelka-Munk absorption spectra and the subspace feature projection.

Table 5: KM-825 Critical Peak Parameters

Wavelength	Peak Amplitude	Full-Width Half-Height
405	0.03	60
475	0.015	40
745	0.26	70
823	0.99	72

KM-832

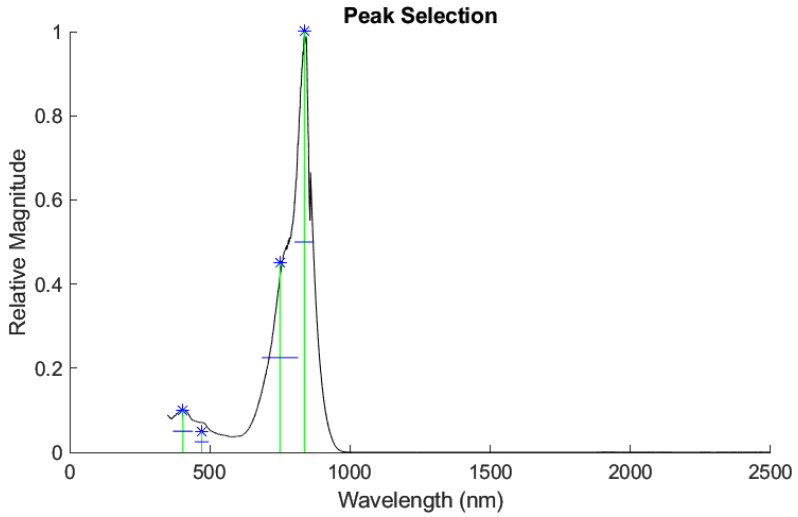

Figure 11: KM-832 absorption spectra and peak characterization.

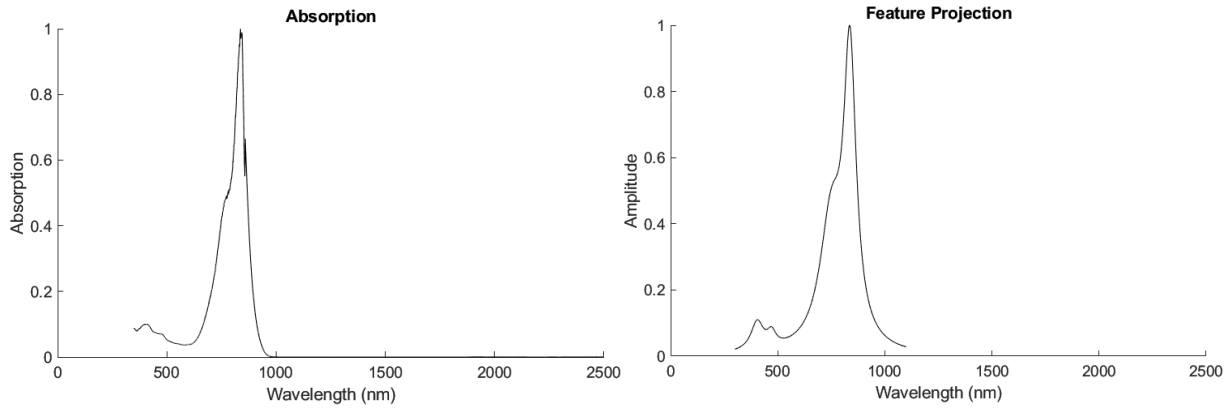

Figure 12: KM-832 comparison between the original Kubelka-Munk absorption spectra and the subspace feature projection.

Table 6: KM-832 Critical Peak Parameters

Wavelength	Peak Amplitude	Full-Width Half-Height
404	0.1	70
471	0.05	50
750	0.45	130
837	1	70

KM-836

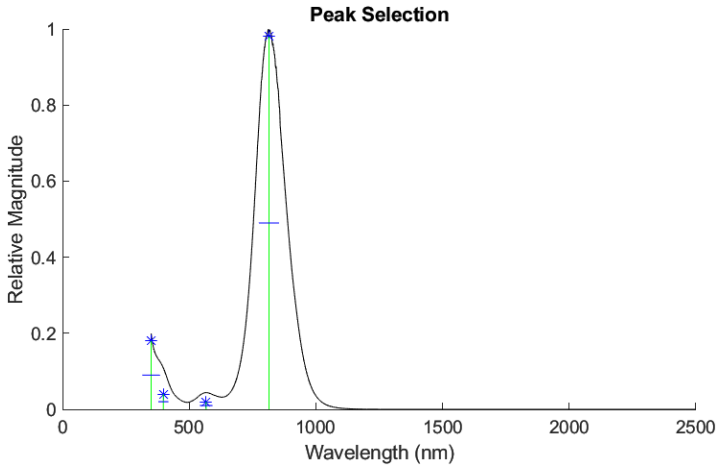

Figure 13: KM-836 absorption spectra and peak characterization.

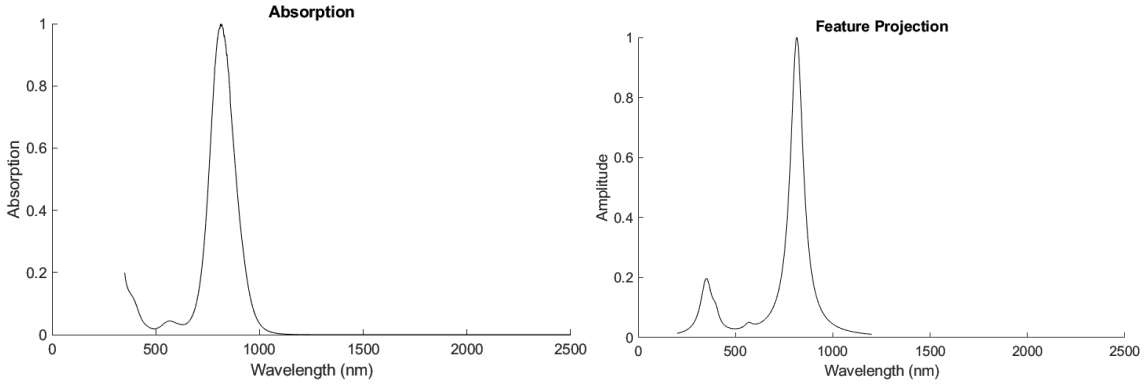

Figure 14: KM-836 comparison between the original Kubelka-Munk absorption spectra and the subspace feature projection.

Table 7: KM-836 Critical Peak Parameters

Wavelength	Peak Amplitude	Full-Width Half-Height
350	0.18	70
398	0.04	40
567	0.02	50
815	0.98	80

KM-845

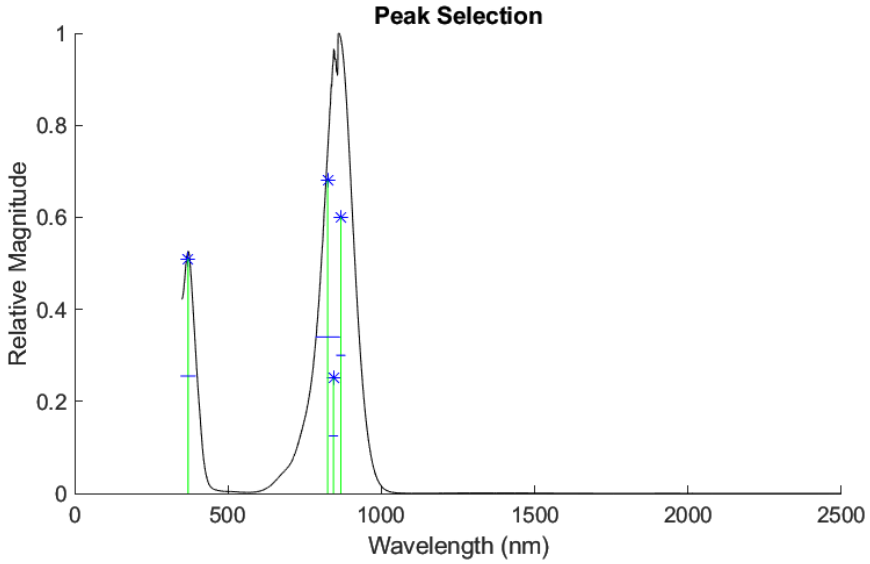

Figure 15: KM-845 absorption spectra and peak characterization.

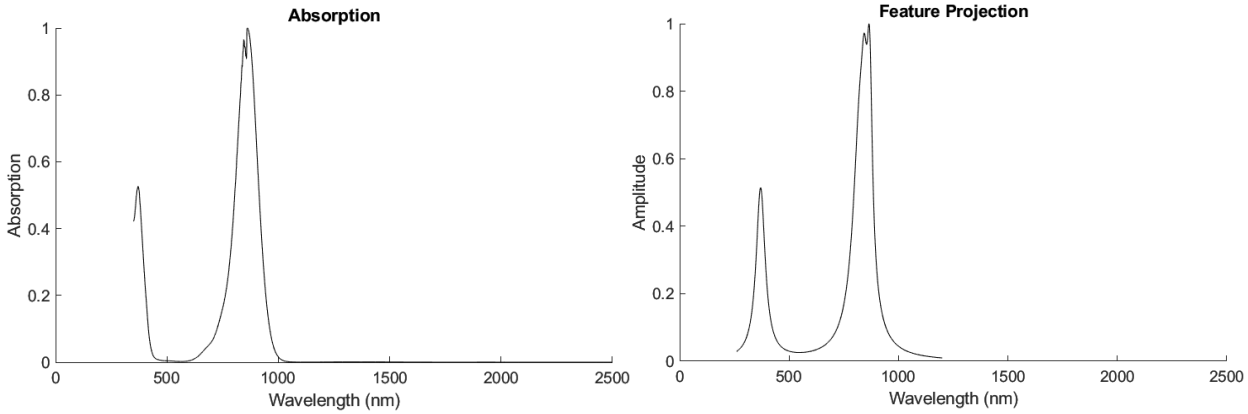

Figure 16: KM-845 comparison between the original Kubelka-Munk absorption spectra and the subspace feature projection.

Table 8: KM-845 Critical Peak Parameters

Wavelength	Peak Amplitude	Full-Width Half-Height
370	0.51	50
825	0.68	80
844	0.25	30
868	0.6	30

KM-848

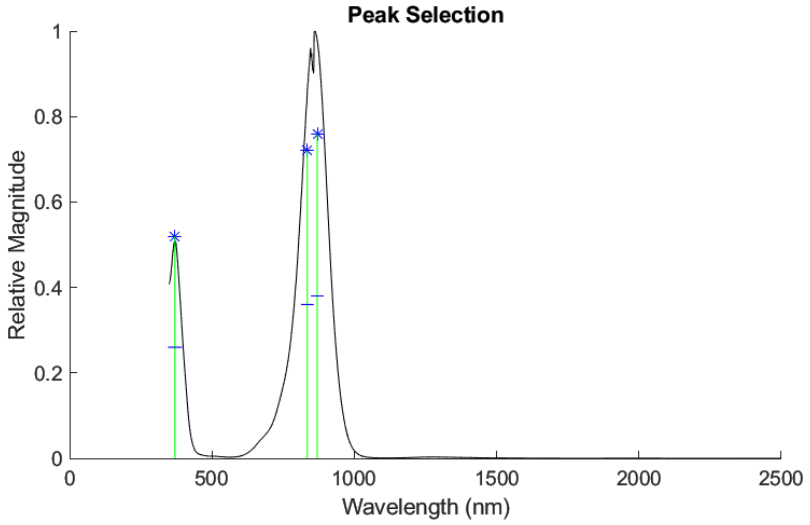

Figure 17: KM-848 absorption spectra and peak characterization.

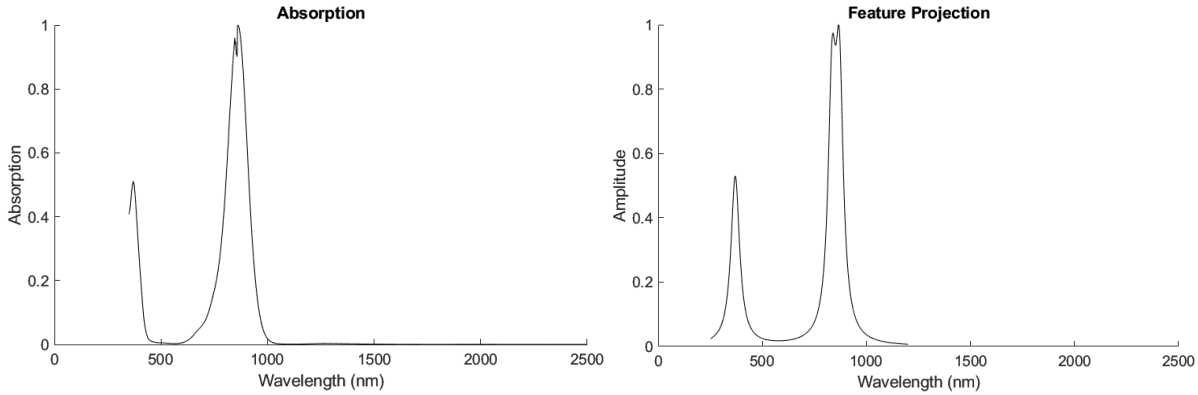

Figure 18: KM-848 comparison between the original Kubelka-Munk absorption spectra and the subspace feature projection.

Table 9: KM-848 Critical Peak Parameters

Wavelength	Peak Amplitude	Full-Width Half-Height
370	0.52	50
835	0.72	45
870	0.76	45

KM-920

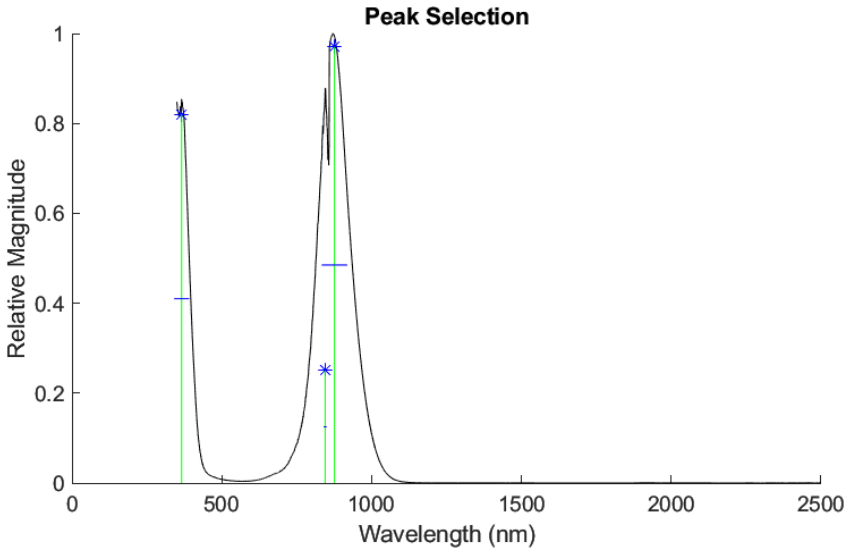

Figure 19: KM-920 absorption spectra and peak characterization.

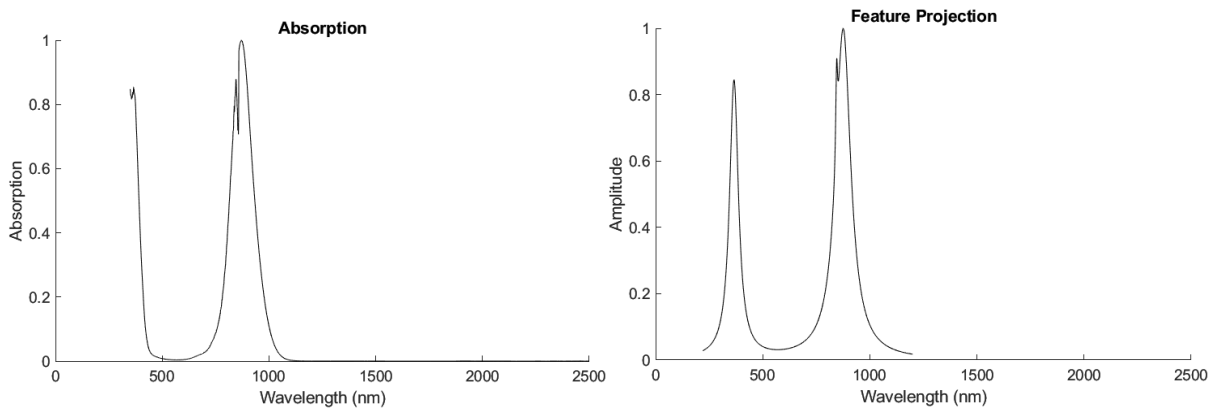

Figure 20: KM-920 comparison between the original Kubelka-Munk absorption spectra and the subspace feature projection.

Table 21: KM-920 Critical Peak Parameters

Wavelength	Peak Amplitude	Full-Width Half-Height
366	0.82	50
845	0.25	10
876	0.97	85

KM-949

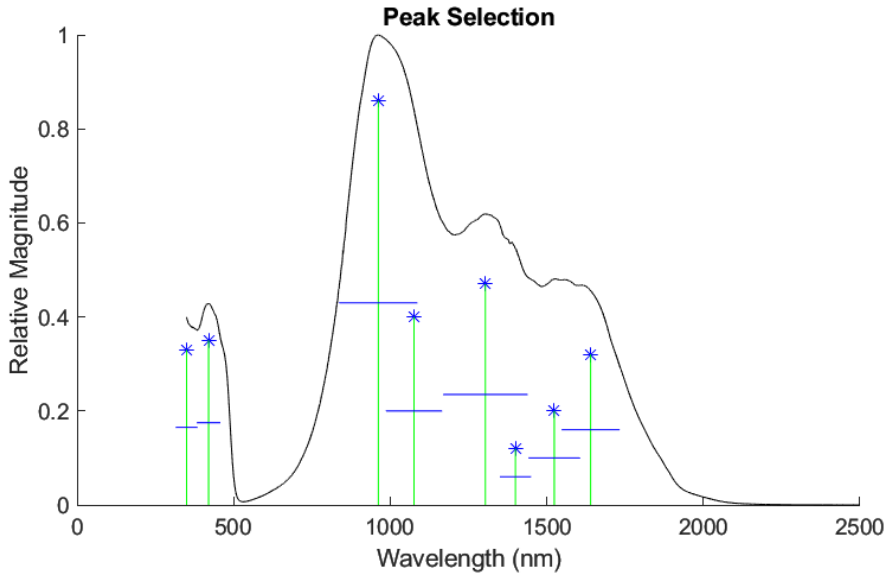

Figure 21: KM-949 absorption spectra and peak characterization.

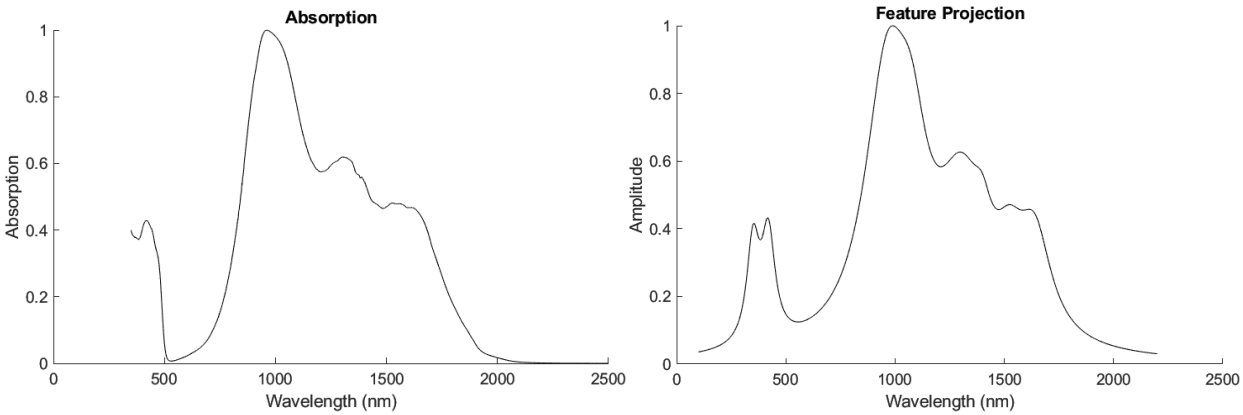

Figure 22: KM-949 comparison between the original Kubelka-Munk absorption spectra and the subspace feature projection.

Table 11: KM-949 Critical Peak Parameters

Wavelength	Peak Amplitude	Full-Width Half-Height
350	0.33	70
420	0.35	75
962	0.86	250
1076	0.4	180
1304	0.47	270
1400	0.12	100
1524	0.2	165
1640	0.32	185

KM-978

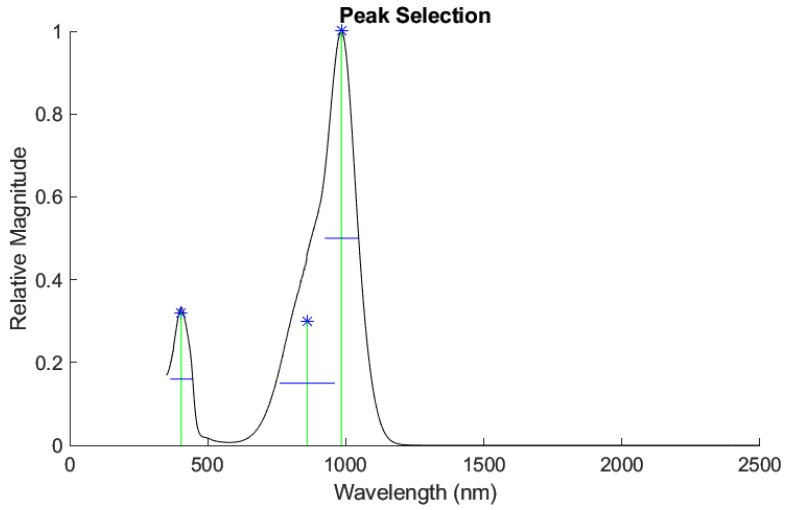

Figure 23: KM-978 absorption spectra and peak characterization.

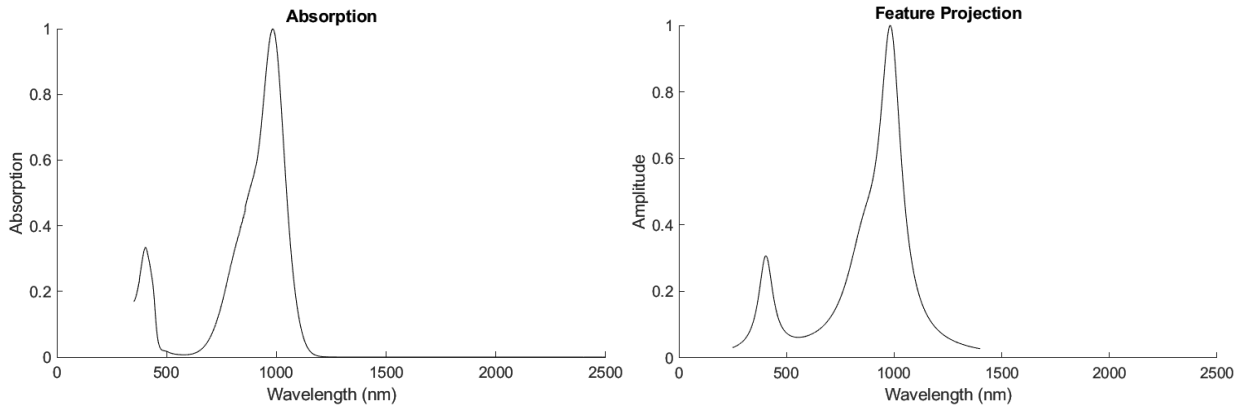

Figure 24: KM-978 comparison between the original Kubelka-Munk absorption spectra and the subspace feature projection.

Table 12: KM-978 Critical Peak Parameters

Wavelength	Peak Amplitude	Full-Width Half-Height
404	0.32	80
860	0.3	200
984	1	120

KM-1072

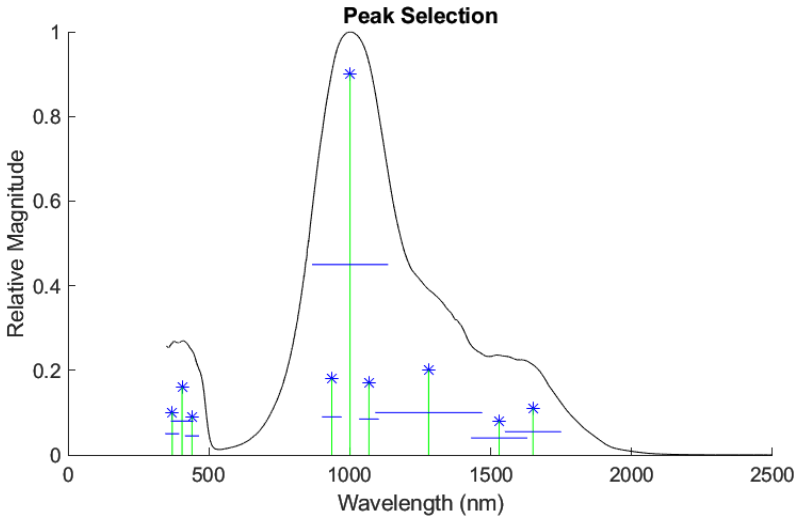

Figure 25: KM-1072 absorption spectra and peak characterization.

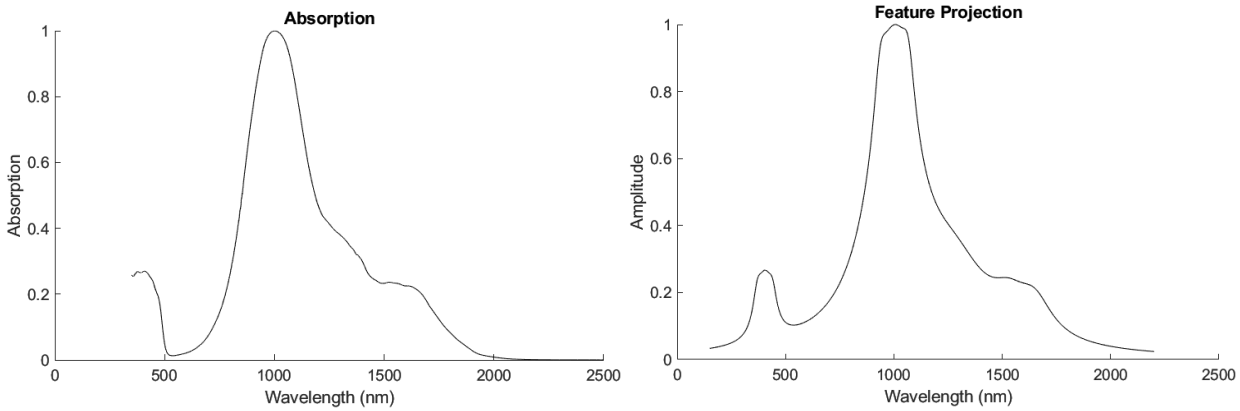

Figure 26: KM-1072 comparison between the original Kubelka-Munk absorption spectra and the subspace feature projection.

Table 13: KM-1072 Critical Peak Parameters

Wavelength	Peak Amplitude	Full-Width Half-Height
370	0.1	50
405	0.16	80
440	0.09	50
936	0.18	70
1001	0.9	270
1068	0.17	70
1280	0.2	380
1530	0.08	200
1650	0.11	200

The complex indices of refraction for the reduced absorption subspaces were estimated and evaluated using Kramers-Kronig analysis (Eq. 9-10). Kramers-Kronig analysis establishes fundamental material properties that can support the characterization of the dielectric response functions. The intermediate index of refraction properties, $\Delta n_N(\lambda)$ and $k_N(\lambda)$, are of particular interest, as they can be scaled – based on the scatterer density – to effectively estimate these dielectric response functions. The Kramers-Kronig results from the reduced subspace absorption were compared to the complex index of refraction for the full dataset with extrapolation, termination, and smoothing corrections, as calculated in reference [14]. The results from these comparisons are shown in Figures 27-38.

KM-720

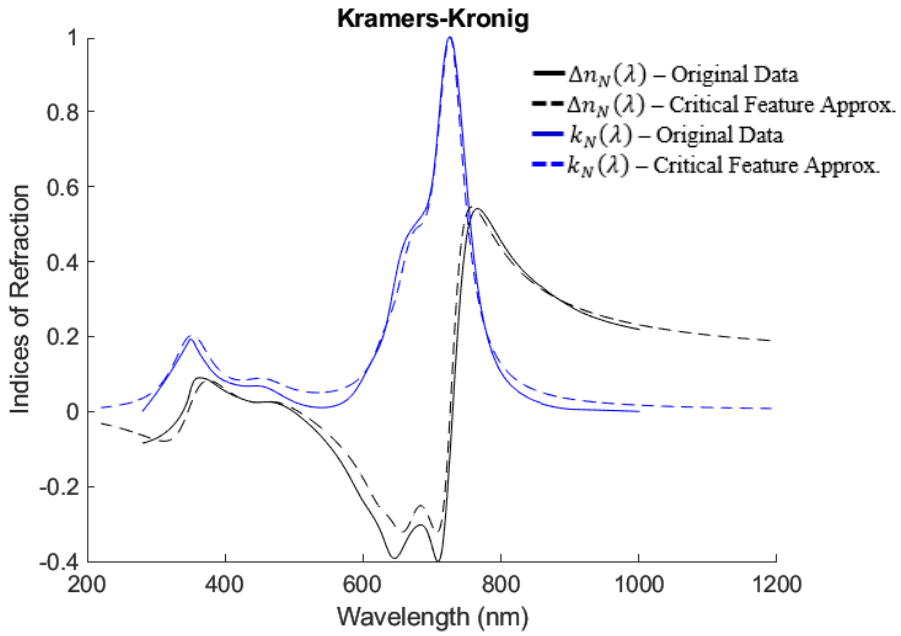

Figure 27: KM-720 Kramers-Kronig indices of refraction, comparing the results from the full extrapolated and smoothed KM dataset with the results from the critical feature approximation.

KM-775

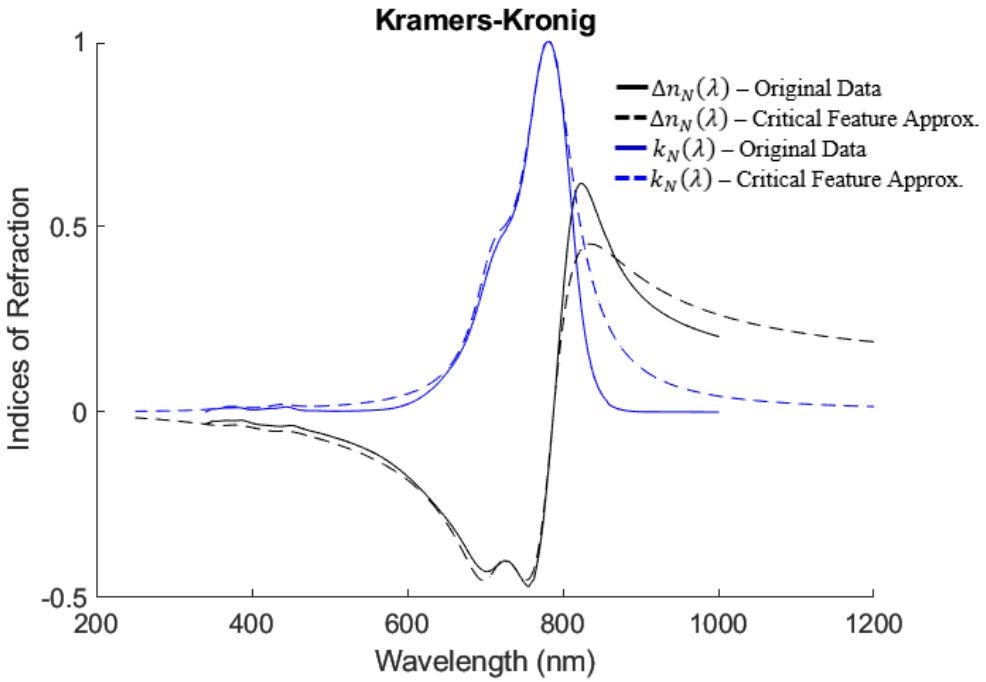

Figure 28: KM-775 Kramers-Kronig indices of refraction, comparing the results from the full extrapolated and smoothed KM dataset with the results from the critical feature approximation.

KM-778

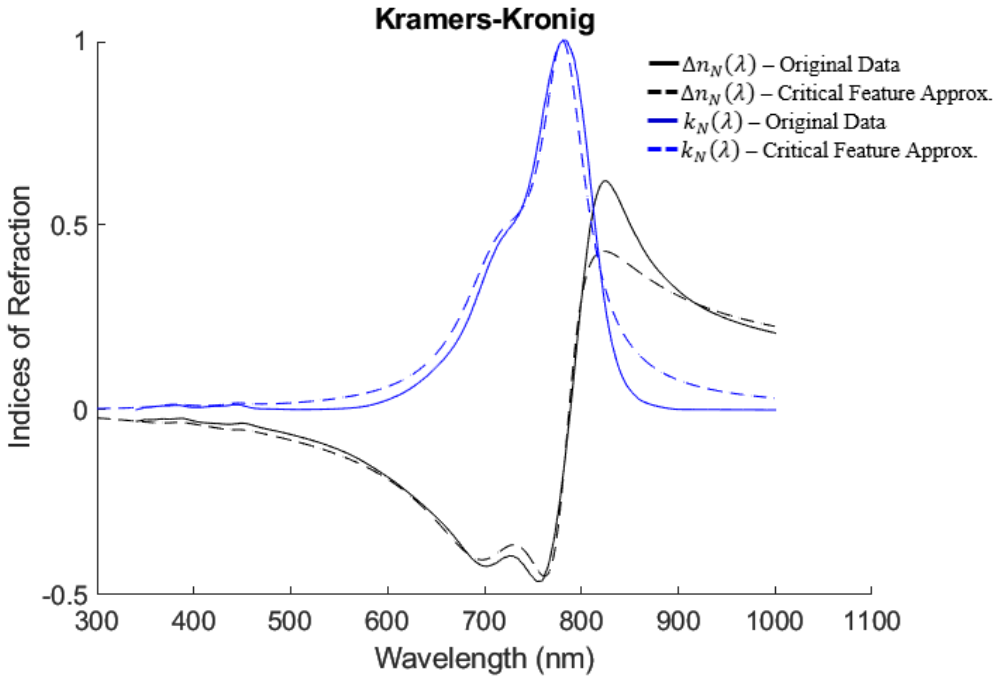

Figure 29: KM-778 Kramers-Kronig indices of refraction, comparing the results from the full extrapolated and smoothed KM dataset with the results from the critical feature approximation.

KM-780

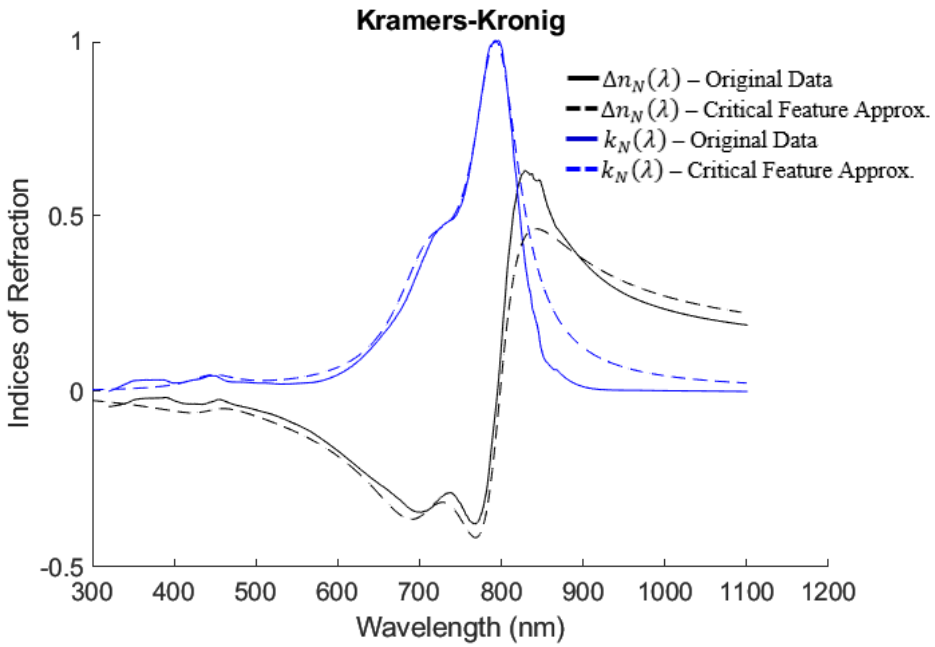

Figure 30: KM-780 Kramers-Kronig indices of refraction, comparing the results from the full extrapolated and smoothed KM dataset with the results from the critical feature approximation.

KM-825

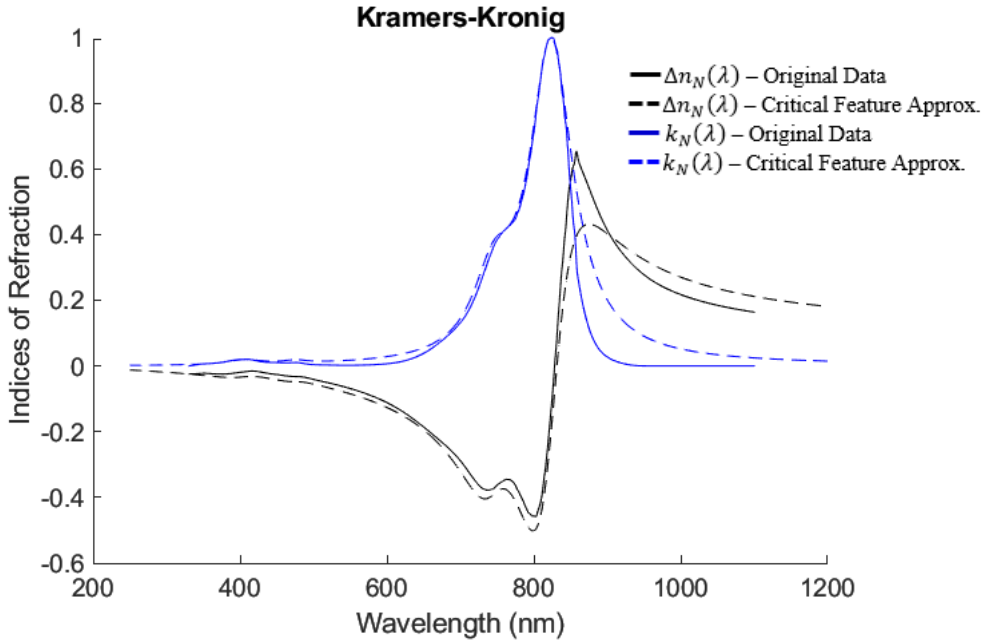

Figure 31: KM-825 Kramers-Kronig indices of refraction, comparing the results from the full extrapolated and smoothed KM dataset with the results from the critical feature approximation.

KM-832

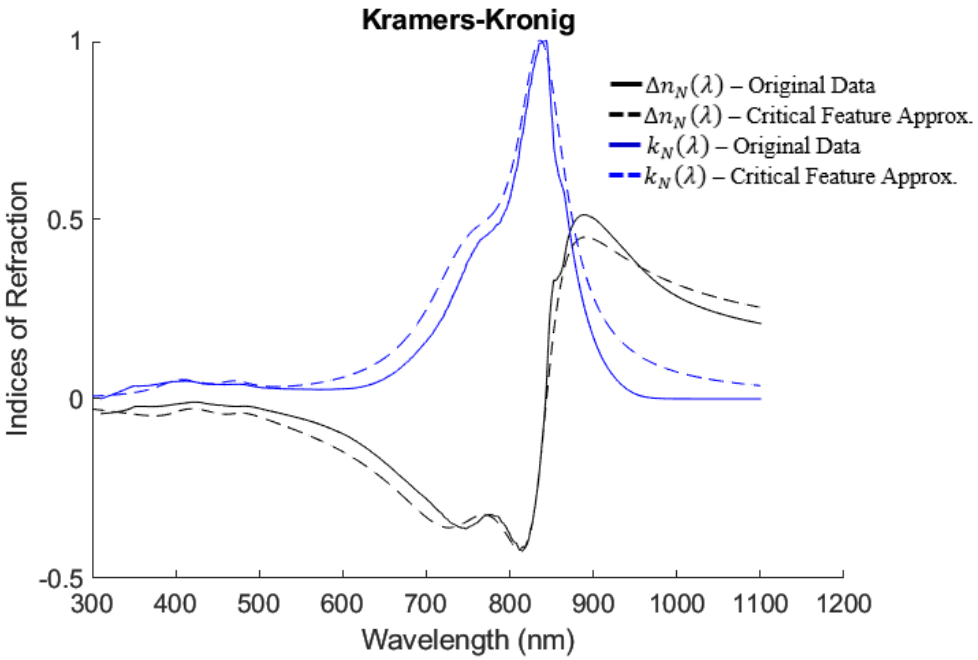

Figure 32: KM-832 Kramers-Kronig indices of refraction, comparing the results from the full extrapolated and smoothed KM dataset with the results from the critical feature approximation.

KM-836

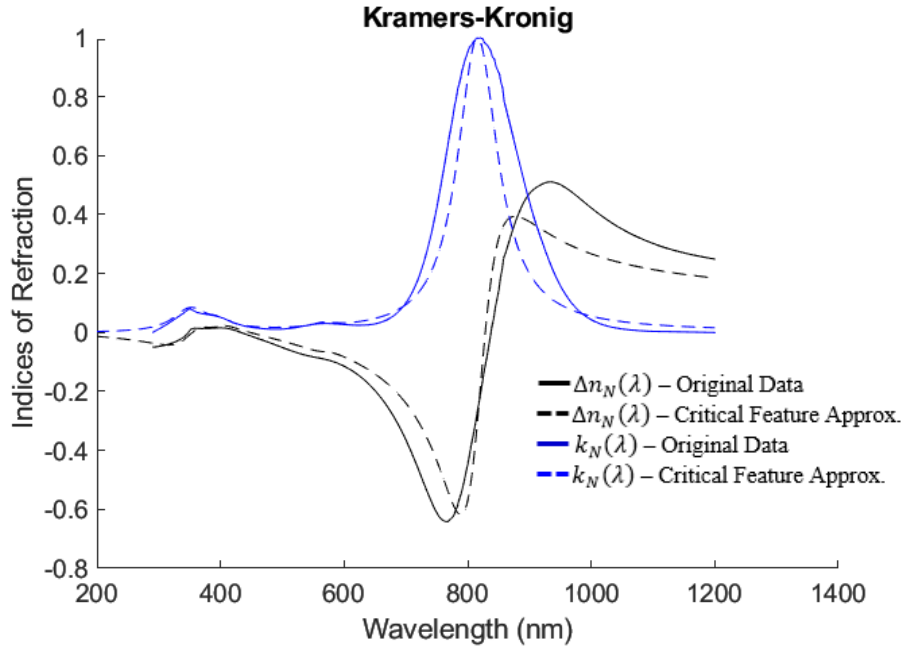

Figure 33: KM-836 Kramers-Kronig indices of refraction, comparing the results from the full extrapolated and smoothed KM dataset with the results from the critical feature approximation.

KM-845

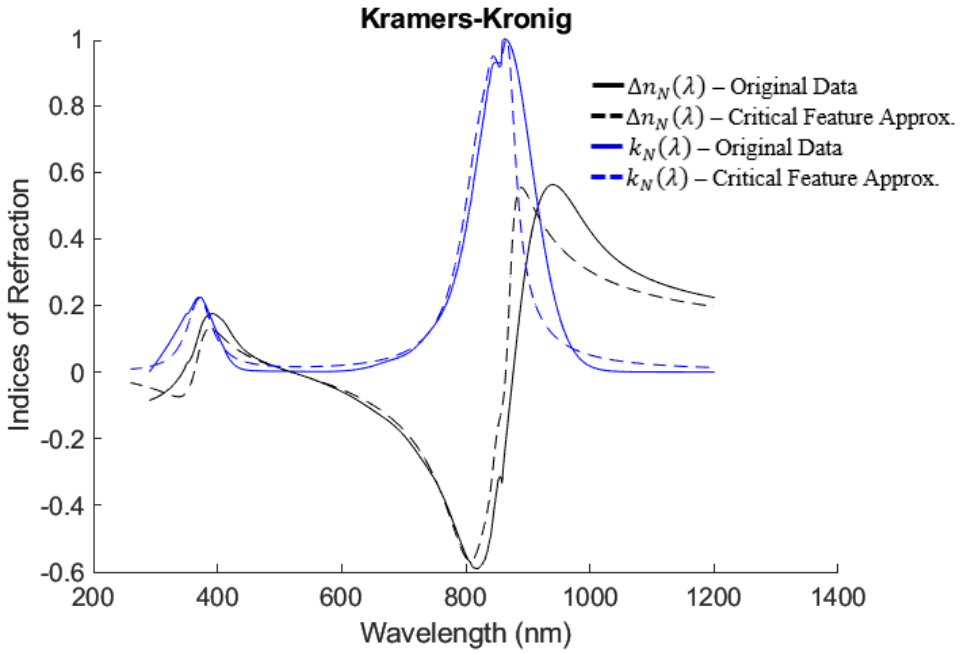

Figure 34: KM-845 Kramers-Kronig indices of refraction, comparing the results from the full extrapolated and smoothed KM dataset with the results from the critical feature approximation.

KM-848

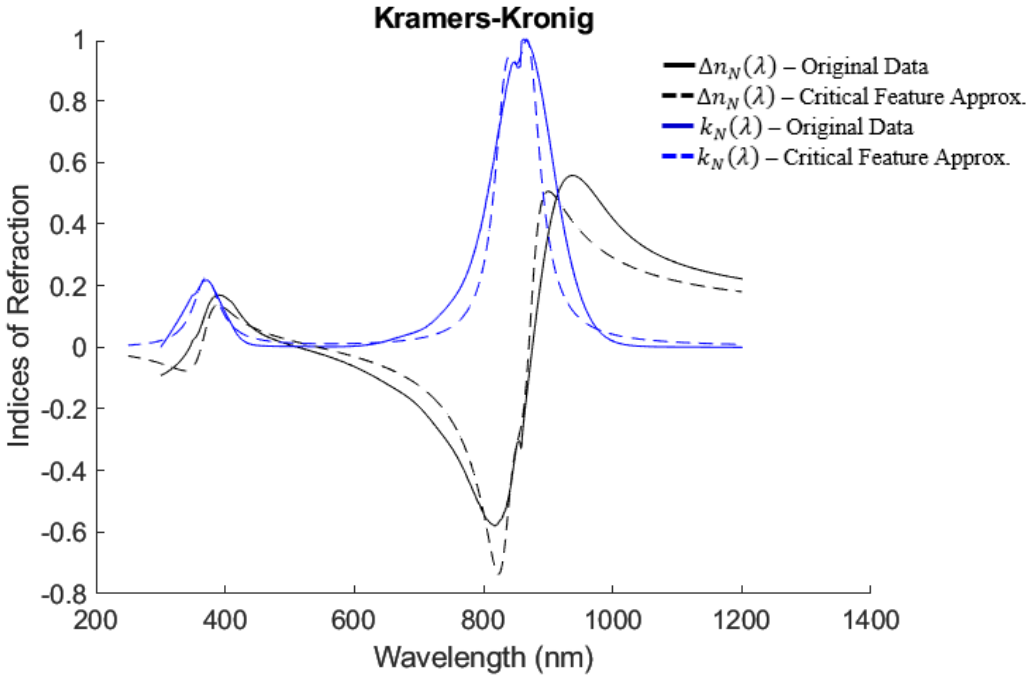

Figure 35: KM-848 Kramers-Kronig indices of refraction, comparing the results from the full extrapolated and smoothed KM dataset with the results from the critical feature approximation.

KM-920

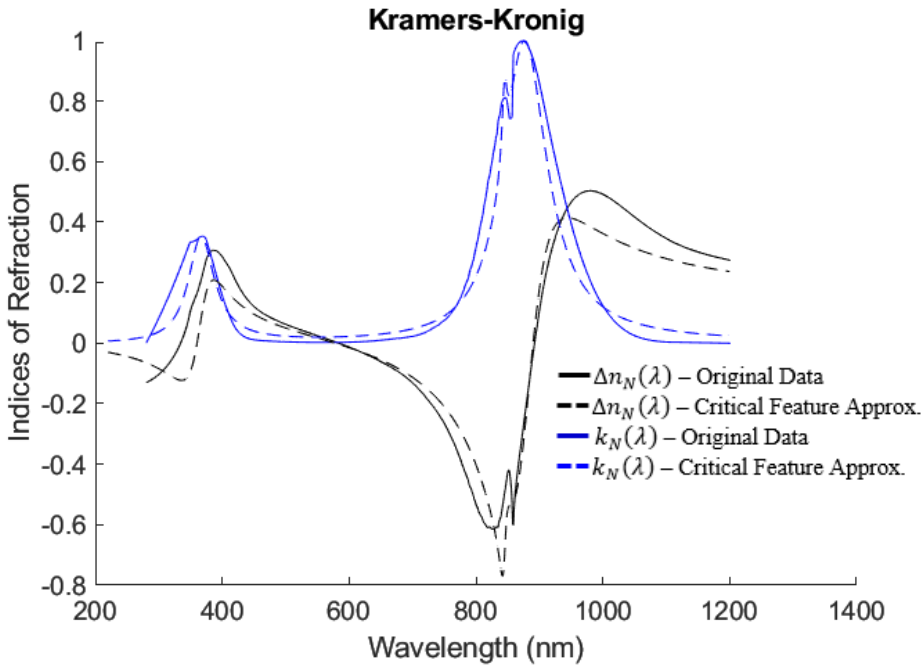

Figure 36: KM-920 Kramers-Kronig indices of refraction, comparing the results from the full extrapolated and smoothed KM dataset with the results from the critical feature approximation.

KM-949

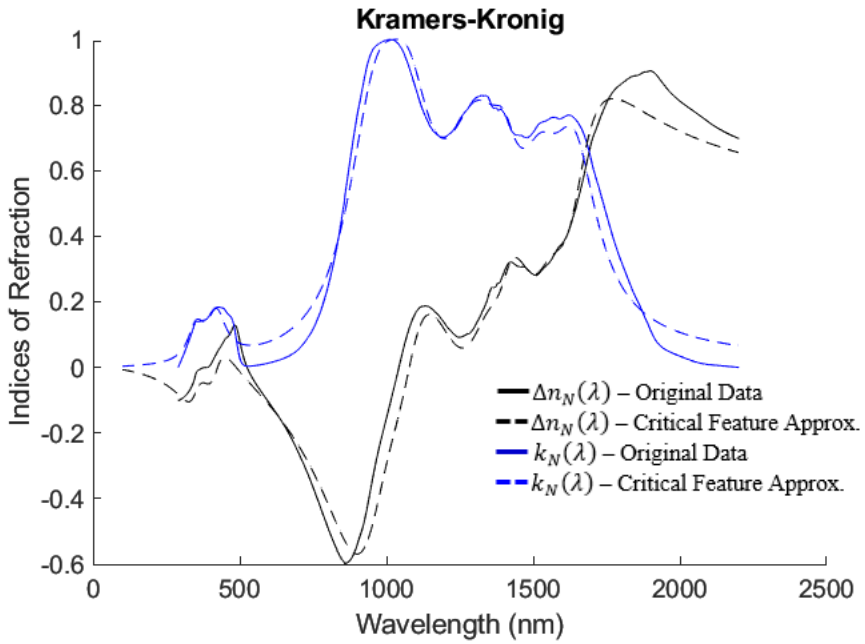

Figure 37: KM-949 Kramers-Kronig indices of refraction, comparing the results from the full extrapolated and smoothed KM dataset with the results from the critical feature approximation.

KM-978

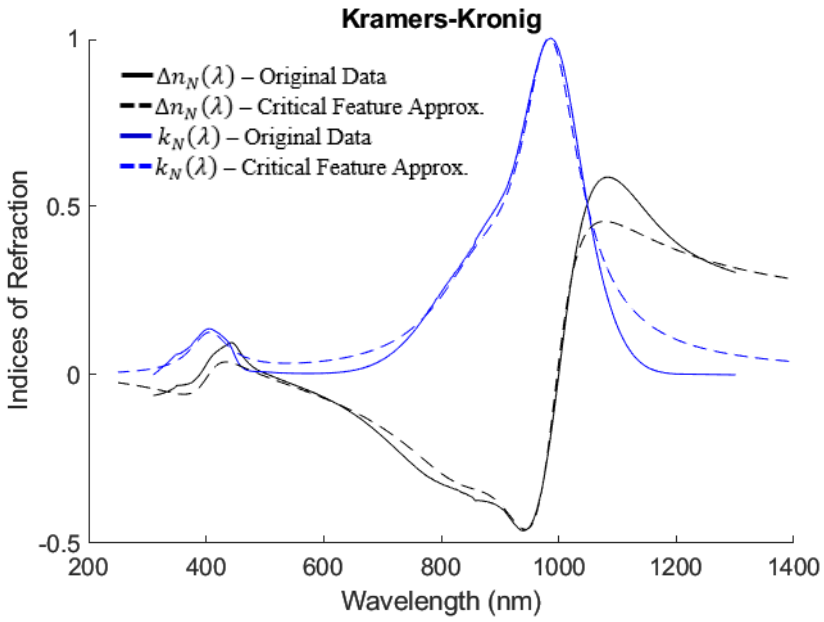

Figure 38: KM-978 Kramers-Kronig indices of refraction, comparing the results from the full extrapolated and smoothed KM dataset with the results from the critical feature approximation.

KM-1072

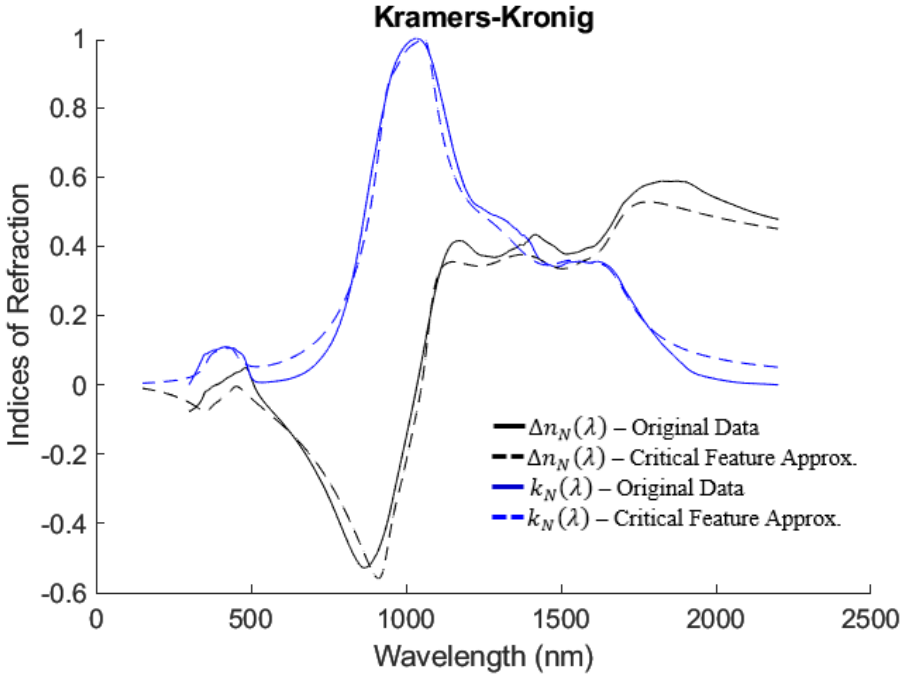

Figure 39: KM-1072 Kramers-Kronig indices of refraction, comparing the results from the full extrapolated and smoothed KM dataset with the results from the critical feature approximation.

Figures 27-39 indicate that the absorption subspaces created from critical feature projection can capture the fundamental characteristics of the Kramers-Kronig indices of refraction, and in-turn the dielectric response behavior. The Kramers-Kronig analysis of the critical feature subspace deviates some in magnitude and width from the full dataset Kramers-Kronig results; however, the critical points of interest within the Kramers-Kronig analysis – including inflection point location – remain similar. This indicates that the underlying dielectric response characteristics are maintained through the reduction of absorption data into a critical feature subspace. Additionally, reduced subspace datasets require no additional extrapolation, termination, or smoothing, unlike the original dataset, which is incomplete in the sense that it does not necessarily approach zero at the lower and upper wavelengths.

Conclusion

The results of this study demonstrate an inverse spectral analysis procedure for determining estimates of dielectric response, which is based on reduction of absorption spectra by means of critical feature isolation and projection. The estimated dielectric response functions can be used to construct a parametric space for developing effective-medium models capable of estimating reflectance from dye formulation on different types of substrates.

Acknowledgements

This project was supported by U.S. DoD programs.

References

1. C.F. Bohren and D.R. Huffman, Absorption and Scattering of Light by Small Particles, Wiley-VCH, 2004.
2. V. Dzimbeg-Malcic, Z. Barbaric-Mikocevic, K. Itric, "Kubelka-Munk Theory in Describing Optical Properties of Paper (I)," Technical Gazette 18, 1 (2011), pp.117-124.
3. P. Kubelka, F. Munk, "Ein Beitrag zur Optik der Farbanstriche," Z. Tech. Phys. (Leipzig), 12 (1931), pp. 593-601.
4. P. Kubelka, "New Contributions to the Optics of Intensely Light-Scattering Materials. Part I," J. Opt. Soc. Am., 38 (1948), pp. 448-457.
5. P. Kubelka, "New Contributions to the Optics of Intensely Light-Scattering Materials. Part II," J. Opt. Soc. Am., 44 (1954), pp. 330-335.
6. D.R. Anifimov, I.G. Golyyak, A.S. Tabalina, I.L. Fufurin, "Kramers-Kronig Relations in Spectral Analysis of Diffuse Reflected Radiation," J. Physics: Conference Series, 1348 (2019) 012084. doi:10.1088/1742-6596/1348/1/012084
7. F.W. King, "Numerical Evaluation of Truncated Kramers-Kronig Transforms," J. Opt. Soc. Am. B, Vol. 24, No. 7 (2007), pp. 1589-1595.
8. M. Bakry and L. Klinkenbusch, "Using The Kramers-Kronig Transforms To Retrieve The Conductivity From The Effective Complex Permittivity," Adv. Radio Sci., 16 (2018), pp. 23-28.
9. K. Ohta and H. Ishida, "Comparison Among Several Numerical Integration Methods for Kramers-Kronig Transformation," Applied Spec., Vol. 42, No. 8 (1988), pp. 952-957.
10. D. Lay, Chapter 7, Linear Algebra and Its Applications (Second Edition), Addison-Wesley, New York (2000), pp. 441-486)

11. R. Viger, S. Ramsey, T. Mayo, S.G. Lambrakos, “Parametric Modeling of Reflectance Spectra for Dyes and Their Mixtures in Fabrics Using Reference Spectra,” Journal of Electromagnetic Waves and Applications, Vol. 33, No. 9, pp. 1163-1171, (2019).
12. Fabricolor Holding International Product List, Laser and Fluorescent dyes, UV and NIR dyes, security inks and other optically functional materials, Code FHI 7206.
13. American Dye Source, Inc., ADS 775PI, CAS # 207399-07-3, 555 Morgan Boulevard, Baie D’Urfe, Quebec, Canada.
14. R. Viger, S.A. Ramsey, T. Mayo, S.G. Lambrakos, “Case-Study Estimation of Dielectric Response Functions for NIR-SWIR Absorbing Dyes by Inverse Analysis of Diffuse Reflectance,” Naval Research Laboratory Memorandum Report, Naval Research Laboratory, Washington, DC, NRL/5708/MR-2022/1, May24, 2022.